SIMULATION OF STRATIFICATION BEHAVIOR OF TWO IMMISCIBLE FLUIDS USING FINITE VOLUME PARTICLE (FVP) METHOD

Faris Kamal Ishlahi[1], Nur Asiah Aprianti*[,1], Asril Pramutadi Andi Mustari[1], and Koji Morita[2]
[1] Nuclear Physics and Biophysics Research Division, Physics Program Study, Faculty of Mathematics and Natural Science, Bandung Institute of Technology (Jalan Ganesha 10, Bandung, West Java 40132, Indonesia)
[2] Department of Applied Quantum Physics and Nuclear Engineering, Kyushu University (744 Motooka, Nishi-ku, Fukuoka 819-0395, Japan)

**** Corresponding author:***
e-mail: asiah@office.itb.ac.id

Received: 29-11-2022
Revision Received: 14-01-2023
Accepted: 09-08-2023
Published: 16-10-2023

DOI : 10.17146/jstni.2023.24.1.6751

Keywords: *Particle Method, FVP, Stratification, Nuclear Reactor.*

Abstract *In this modern era, the need for energy is increasing, and the environmental issues caused by the energy industry are also increasing. Therefore, one of the long-term alternative energy sources is nuclear energy. However, as is well known, there have been many nuclear reactor accidents, such as the Chernobyl, Three Miles Island, and Fukushima reactors. In those cases, there was an accident in the core reactor, especially the melting of the reactor core. One phenomenon is the stratification of the molten metal component of the melted reactor core. Using simulation, this study will discuss the stratification behavior of two immiscible and incompressible fluids. The particle-based simulation method has advantages over the mesh method in simulating free surface conditions and has a lighter computational load. The particle method used in this simulation is the Finite Volume Particle (FVP) method, derived based on the finite volume method by assuming each particle occupies a certain volume. The simulation of the stratification behavior is carried out using three types of fluids, water, cooking oil, and lubricating oil, which are combined into three variations. The stratification simulation results will be compared with the experimental results obtained from the reference. From the simulation results obtained, there is a pattern similar to the experimental results. Simulation data is also processed to obtain the penetration ratio between fluids in each variation and the length of water penetration through cooking and lubricating oil. The results show that the magnitude of the difference in fluid density and viscosity affects the stratification process.*

INTRODUCTION

In nuclear physics, particularly within nuclear reactors, many fluid phenomena manifest. Nuclear reactors, serving as energy generators, involve intricate fluid cycles. These reactors employ diverse fluids, ranging from water and liquid metals to molten salt solutions, each contingent on the reactor type. Notably, during reactor incidents like core meltdowns, many fluid phenomena transpire, including the stratification of reactor core melt (1–4). Such stratification arises from variations in fluid density, causing denser fluid to underlie less dense fluid, resulting in a stratified fluid with density increment along its depth (5). However, the experimental investigation of severe accident stratification often necessitates considerable resources due to high-temperature conditions. To address this resource challenge, computational simulations have emerged as a viable solution, having found application in nuclear severe accident research for years. Noteworthy approaches include mesh-based methods, exemplified by Tran et al.'s utilization of computational fluid dynamics (CFD) (6) to create effective safety analysis tools, presented by their work on studying molten corium coolability in a BWR lower head. Another avenue involves particle-based methods, harnessing their capacity to address surface deformations. Asril et al., for instance, performed simulations to study severe accidents, validating their approach against simple experiments (7–10).

Analyzing complex problems through analytical methods often entails substantial effort. Using numerical approaches facilitated by computer-based simulations offers an efficient solution. The Finite Volume Particle (FVP) method incorporates particle concepts among the diverse numerical methods employed for dynamic fluid modeling. As Aprianti N. A. et al. (11) exemplified, this method leverages particle-based modeling to alleviate the computational load associated with mesh generation. Furthermore, integrating finite volume principles restricts particle interactions with neighboring particles, curtailing the extent of necessary numerical computations. Particularly

advantageous for various fluid phenomena modeling, the FVP method captures intricate dynamics such as fluid stratification, a focal point of this study as highlighted by Yulianto Y. et al. (5).

In this investigation, the FVP source code underwent tailored modifications to replicate the stratification dynamics of two immiscible fluids. The validation process encompassed an experiment involving three commonplace immiscible liquids—water, cooking oil, and lubricant oil—drawn from Y. Yulianto et al.'s 2018 scientific publication (5). Furthermore, the simulations explored the impact of varying densities and viscosities of the liquids, delving into their effects on the overall behavior.

METHODOLOGY

Finite Volume Particle (FVP) Method

The FVP method uses numerical particles to discretize the governing equations. This numerical particle is assumed to fulfill a certain volume. The volume control of a moving particle is a circle in a 2D simulation (N. A. Aprianti et al., 2015),

$$S = 2\pi R \ \ , V = \pi R^2 = (\Delta l)^2. \quad (1)$$

Where S, V, R, and Δl are the surface area, particle volume control, particle volume control radius, and initial particle distance, respectively.

Based on Gauss's law, the gradient and Laplacian operators apply to arbitrary scalar functions, which are expressed by the following equation,

$$\nabla\phi = \lim_{R\to 0}\frac{1}{V}\oint_V \ \nabla\phi dV = \lim_{R\to 0}\frac{1}{V}\oint_S \ \phi\bar{n}dS \quad (2)$$

$$\nabla^2\phi = \lim_{R\to 0}\frac{1}{V}\oint_V \ \nabla^2\phi dV = \lim_{R\to 0}\frac{1}{V}\oint_V \ \nabla\phi\cdot\bar{n}dS \quad (3)$$

Using the FVP method, gradient, and Laplacian term from *i* th particle can be approximated with the equation given below,

$$\langle\nabla\phi\rangle_i = \langle\frac{1}{V}\oint_S \ \phi\bar{n}dS\rangle_i = \frac{1}{V}\sum_{j\neq i}\phi_{sur}\cdot\bar{n}_{ij}\cdot\Delta S_{ij} \quad (4)$$

$$\langle\nabla^2\phi\rangle_i = \langle\frac{1}{V}\oint_S \ \nabla\phi\cdot\bar{n}dS\rangle_i = \frac{1}{V}\sum_{j\neq i}\left(\frac{\phi_j-\phi_i}{|\vec{r}_{ij}|}\right)\cdot\Delta S_{ij} \quad (5)$$

Where $|\vec{r}_{ij}|$ is the distance between *i* and *j* particles, ϕ_{sur} is the reconstruction value of arbitrary functions on the surface of *i* particle. while, $\langle\phi\rangle_i$ is the approximate result of ϕ, $\bar{n}_{ij}$ is the unit vector of the distance between *i* particle and *j* particle, and ΔS_{ij} surface interaction of *i* and *j* particles.

The value of the surface function (ϕ_{sur}) can be evaluated using a linear function which can be shown in the following equation,

$$\phi_{sur} = \phi_i + \frac{\phi_j-\phi_i}{|\vec{r}_{ij}|}R \quad (6)$$

then the unit vector $\bar{n}_{ij}$ at a distance between *i* and *j* particles can be represented as the equation below,

$$\bar{n}_{ij} = \frac{\vec{r}_{ij}}{|\vec{r}_{ij}|} = \frac{(\vec{r}_j-\vec{r}_i)}{|\vec{r}_{ij}|}. \quad (7)$$

For the surface interaction function between *i* and *j* particles, ΔS_{ij}, can be estimated as in the equation written below,

$$\Delta S_{ij} = \frac{\omega_{ij}}{\sum_{j\neq i}\omega_{ij}}S \quad (8)$$

where the ω_{ij} term is kernel function that can be defined below,

$$\omega_{ij} = \begin{cases} \sin^{-1}\left(\frac{R}{|\vec{r}_{ij}|}\right) - \sin^{-1}\left(\frac{R}{r_e}\right) & ,|\vec{r}_{ij}| \leq r_e \\ 0 & ,|\vec{r}_{ij}| \geq r_e. \end{cases} \quad (9)$$

Where r_e is the selected cut-off radius *Δl* for the 2D system. The cut-off radius is the boundary area of the neighboring particles around *i* particle. This neighboring fluid-particle interaction is used in modeling the movement/displacement of particles. The scheme for the interaction of particles with neighboring particles can be shown in Fig.1 below,

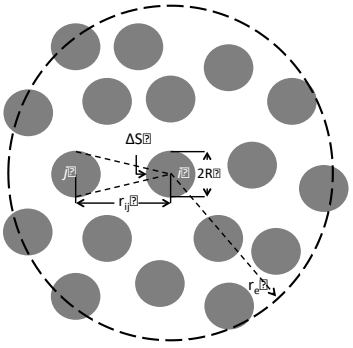

Figure 1. Scheme of neighboring particles around i particle in the ring of cut-off radius

Governing Equations

The governing equation used for this simulation of Rayleigh-Taylor instability for incompressible fluid is the Navier-Stokes equation and continuity equation; those equations are given below,

$$\begin{cases} \rho\frac{D\vec{u}}{Dt} = -\nabla p + \nabla(\mu\nabla\cdot\vec{u}) + \overrightarrow{f_s} + \overrightarrow{f_g} \\ \nabla\cdot\vec{u} = 0 \end{cases} \quad (10)$$

Where ρ is the density of the fluid, $\vec{u}$ is velocity, t is for time, p is pressure, and μ is dynamic

viscosity. The $\vec{f}$ terms on the right side of the Navier-Stokes equation are force per volume units such as gravity and surface tension.

Algorithm

An algorithm is needed to calculate the simulation using the method correctly. The algorithm used for this simulation is an explicit-implicit algorithm with less computation load, so do shorten the computation time. The algorithm diagram is shown in figure 2.

When at the explicit step, the temporary velocity of the particles is explicitly updated with viscosity, surface tension, and external forces using the following equation,

$$\vec{u}^* = \vec{u}^n + \Delta t\left[\frac{1}{\rho}\nabla\hat{\mu}\cdot\nabla\vec{u}^n + \frac{\hat{\mu}}{\rho}\nabla^2\vec{u}^n + \vec{g} + \vec{f}^n\right] \quad (11)$$

After that, temporary positions of the particles will also be updated explicitly using following equation,

$$\vec{r}^* = \vec{r}^n + \Delta t\vec{u}^*. \quad (12)$$

Then at the update step, velocity and position of particles can be solved using equation below,

$$\vec{\mathrm{u}}^{\mathrm{n+1}} = \vec{\mathrm{u}}^* - \Delta\mathrm{t}\frac{1}{\rho}\nabla\mathrm{p}^{\mathrm{n+1}}. \quad (13)$$

$$\vec{\mathrm{r}}^{\mathrm{n+1}} = \vec{\mathrm{r}}^{\mathrm{n}} + \Delta\mathrm{t}\vec{\mathrm{u}}^{\mathrm{n+1}}. \quad (14)$$

Before that, the implicit step will be solved the pressure poisson equation using a method called Combine Unified Procedure (CUP). Using this CUP method, the change of pressure can be related to density using a new term, sound velocity, to reduce the implicitness of the pressure. Firstly, from the continuity equation can be derived as follow,

$$\frac{D\rho}{Dt} = -\rho\nabla\cdot\vec{u}. \quad (15)$$

which then can be rearranged into the following equation,

$$\nabla\cdot\vec{u} = -\frac{1}{\rho}\frac{D\rho}{Dt} = -\frac{1}{\rho}\frac{\partial\rho}{\partial p}\frac{Dp}{Dt} - \frac{1}{\rho}\frac{\partial\rho}{\partial e}\frac{De}{Dt}. \quad (16)$$

where e is internal energy. For incompressible flow, heat conduction and dissipation do not occur, so we have

$$\frac{De}{Dt} = 0. \quad (17)$$

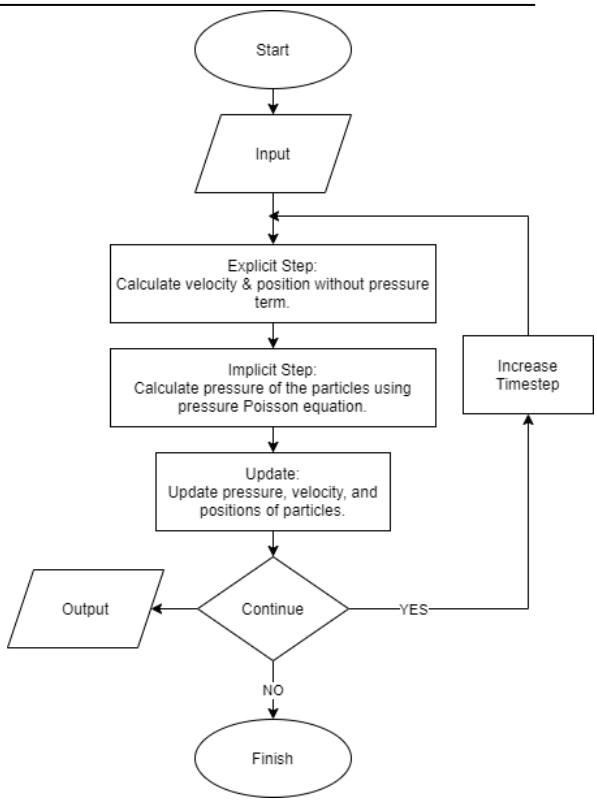

Figure 2. Explicit-Implicit algorithm diagram.

Furthermore, sound velocity can be expressed by the following equation,

$$c_s{}^2 = \frac{\partial p}{\partial\rho}. \quad (18)$$

where $c_s{}^2$ is smoothed square value of sound velocity. From Eq.17 and Eq.18, the Eq.16 can be rewritten to be the following equation,

$$\nabla\cdot\vec{u} = -\frac{1}{\rho c_s{}^2}\frac{Dp}{Dt}. \quad (19)$$

Then the above equation (Eq.19) can be expressed as,

$$\nabla\cdot\vec{u}^{n+1} = -\frac{1}{\rho c_s{}^2}\frac{p^{n+1}-p^n}{\Delta t}. \quad (20)$$

Also, the Eq.13 can be expressed as follow,

$$\nabla\cdot\vec{u}^{n+1} = \nabla\cdot\vec{u}^* - \nabla\cdot\left(\Delta t\frac{1}{\rho}\nabla p^{n+1}\right). \quad (21)$$

Then Eq.20 and Eq.21 can be combined and resulting in the following equation,

$$-\frac{1}{\rho c_s{}^2}\frac{p^{n+1}-p^n}{\Delta t} = \nabla\cdot\vec{u}^* - \frac{\Delta t}{\rho^2}\nabla\rho\cdot\nabla p^{n+1} - \frac{\Delta t}{\rho}\nabla^2 p^{n+1}. \quad (22)$$

To get a symmetry equation, Eq.22 can be changed into the following equation,

$$-\frac{1}{\rho c_s{}^2}\frac{p^{**}-p^*}{\Delta t} = \nabla\cdot\vec{u}^* - \frac{\Delta t}{\rho^2}\nabla\rho\cdot\nabla p^* - \frac{\Delta t}{\rho}\nabla^2 p^*. \quad (23)$$

where p^* is the initial p value that is equalized with p^n, and p^{**} can be solved using

Eq.23. After the value of p^{**} is obtained, the value will be given to p^{*} and then p^{**} will be solved again until the value of p^{*} and p^{**} are become convergent. The convergent value will be given to p^{n+1}, then the rest can be solved using Incomplete Cholesky Conjugate Gradient (ICCG) algorithm (11).

Simulation Geometry

To initiate the simulation, specific parameters are employed to model the phenomenon utilizing the FVP method. The simulation involves three distinct fluids: water, cooking oil, and lubricant oil. Table 1 presents comprehensive data pertaining to these fluids.

Table 1. Data parameter of the fluid used for the simulation

Parameter	Variation 1		Variation 2		Variation 3	
	Fluid 1	Fluid 2	Fluid 1	Fluid 2	Fluid 1	Fluid 2
	Cooking Oil	Water	Lubricant Oil	Water	Lubricant Oil	Cooking Oil
Density(kg/m^3)	890.13	1000	848.30	1000	848.30	890.13
Viscosity (Pa.s)	4.73e^{-2}	1.00e^{-3}	12.19e^{-2}	1.00e^{-3}	12.19e^{-2}	4.73e^{-2}

The initial condition of the fluid particles in the simulation, when the simulation time is zero (t=0), is given below for the position of the fluid particles. We consider wall and free surface boundary conditions as explained in previous works (11)

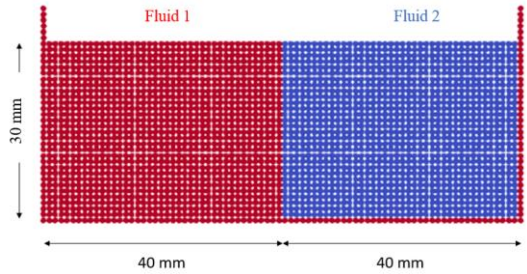

Figure 3. Geometrical condition.

RESULTS AND DISCUSSION

We simulated three different fluid variations (as presented in Table 1) to observe their respective stratification behaviors. The obtained simulation outcomes were subsequently compared to the experimental findings conducted by Y. Yulianto et al. in 2018 (5), visualized in Figures 4, 5, and 6.

The simulation results exhibit a notable resemblance to the experimental outcomes. Each variant attains stratified conditions at distinct time points. Notably, the variant involving cooking oil and lubricant oil indicates a comparatively lengthier duration to achieve stratification, whereas the other two variants manifest a minor disparity in their stratification timing.

Consistent with earlier assertions, the simulation pattern closely mirrors the experimental behavior. Notably, each variant exhibits a distinctive duration to attain stratified conditions. We calculate the penetration distance ratio and present it graphically to analyze the impact further.

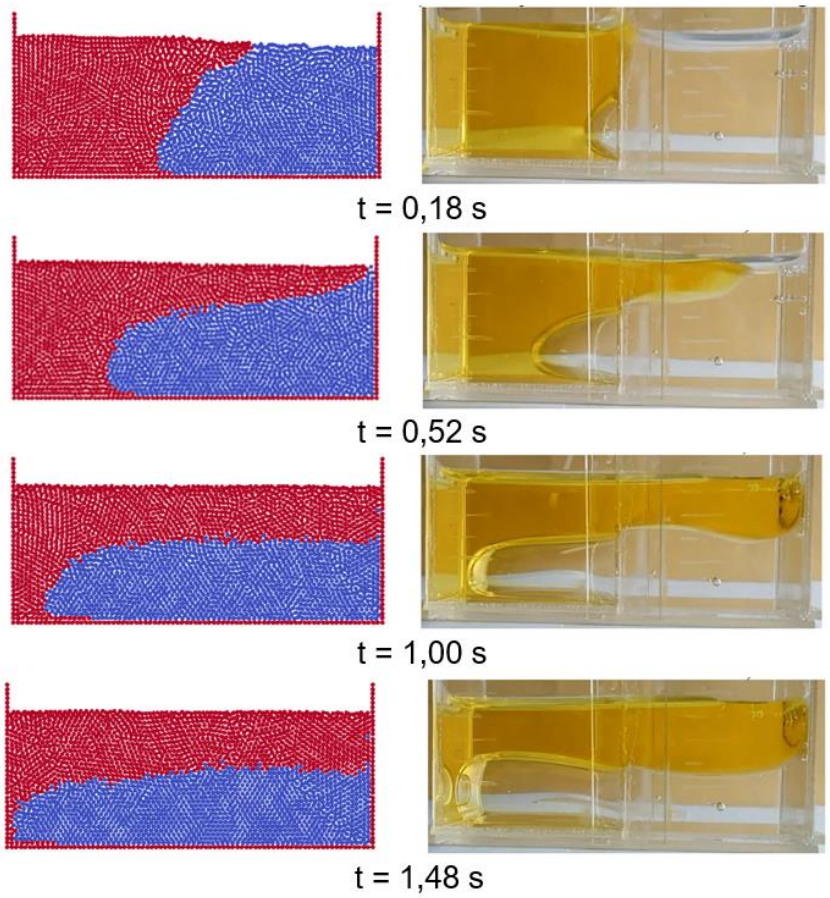

Figure 4. Simulation result (left) and experiment (right) for variation 1 (5).

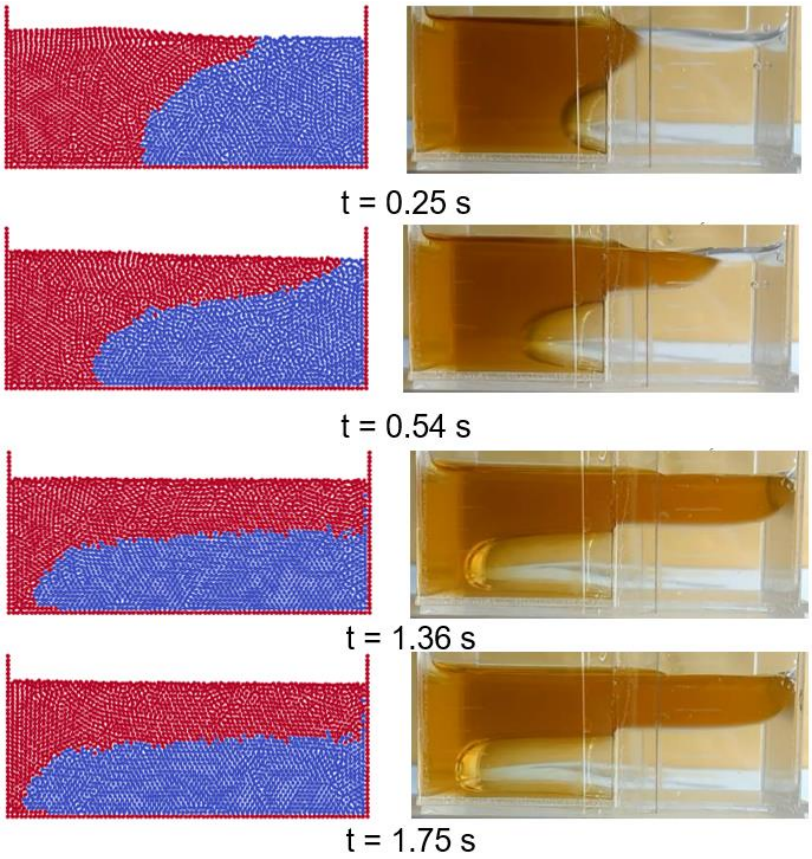

Figure 5. Simulation result (left) and experiment (right) for variaton 2 (5).

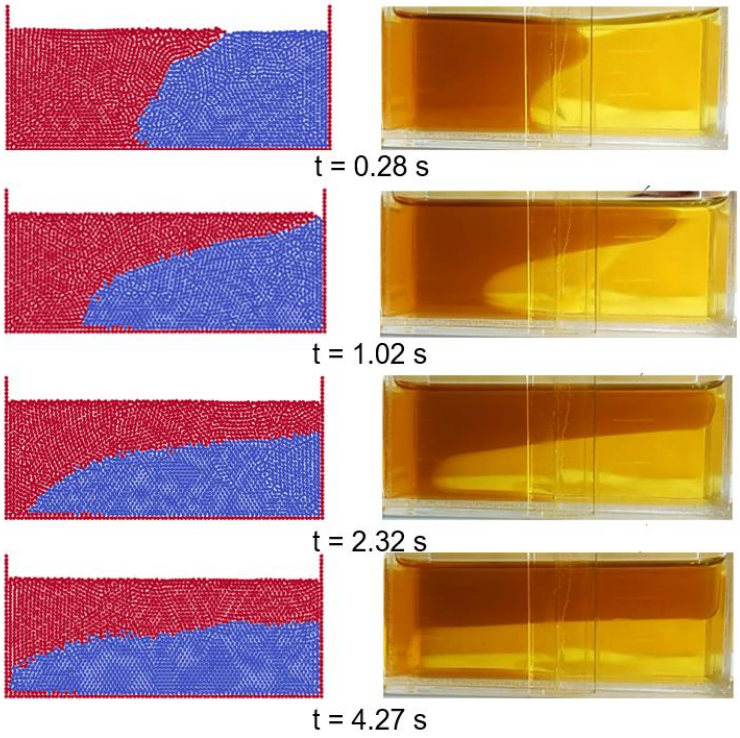

Figure 6. Simulation result (left) and experiment (right) for variation 3 (5).

The analysis of the graphical representations in Figures 7 and 8 reveals a discernible pattern: at the outset, a ratio exceeding unity indicates that Fluid 2, represented by water in these scenarios, exhibits a deeper penetration than Fluid 1. Subsequently, this ratio steadily diminishes as Fluid 1 accelerates its movement at a pace surpassing that of Fluid 2, ultimately converging to a ratio of zero as the system achieves stratification. Interestingly, Figure 9 offers a distinct perspective in the third variation, where the initial ratio begins below one, signaling that Fluid 1's penetration velocity outpaces Fluid 2 right from the commencement. This intriguing variation between the simulation and the experiment stems from the mechanics of the experimental setup, where the separator's lifting introduces a time lag, causing the fluid at the top to initiate its penetration or motion later than its lower counterpart. In contrast, the simulation environment lacks a separator, enabling unrestricted fluid movement and immediate penetration.

Furthermore, the analysis extends to encompass water penetration rates within other fluids, namely cooking oil and lubricant oil, enabling an insightful exploration into the impact of viscosity. A comprehensive understanding of viscosity's influence is achieved by plotting a time-to-penetration distance graph, illuminating the intricate behavior of the water penetration rate across different conditions.

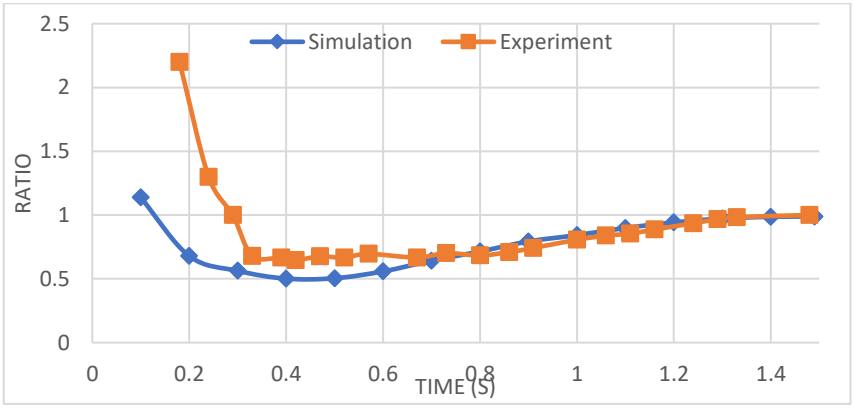

Figure 7. Ratio of penetration length for cooking oil and water.

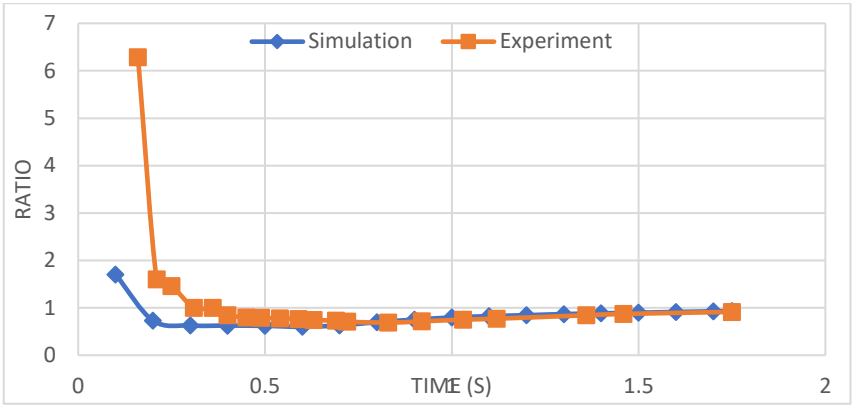

Figure 8. Ratio of penetration length for lubricant oil and water.

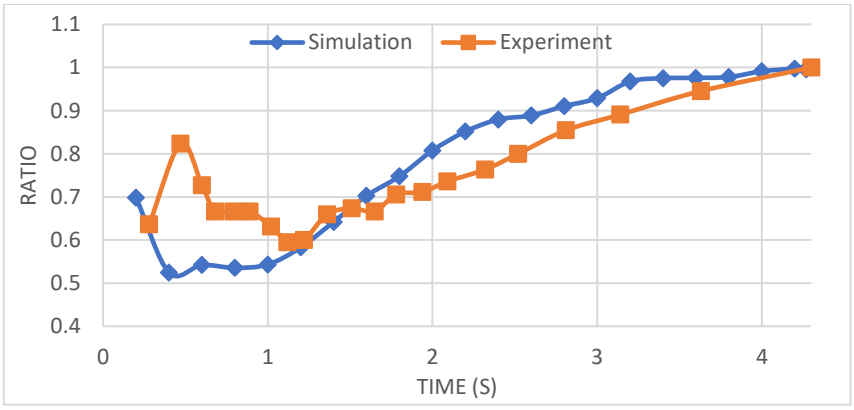

Figure 9. The ratio of penetration length for cooking oil and lubricant oil.

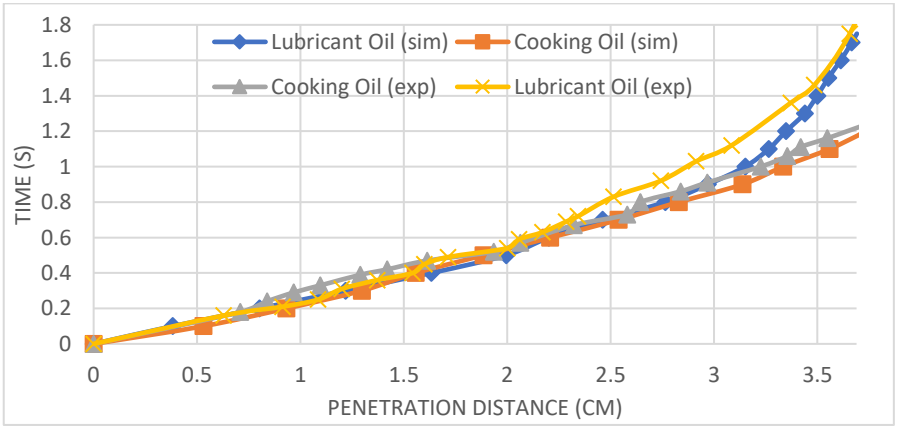

Figure 10. The water penetration rate in cooking oil and lubricant oil.

Figure 10's graph provides a revealing insight: both in simulation and experiment, the time required for stratification in lubricant oil surpasses that in cooking oil. This observation implies that water achieves swifter cooking oil penetration than denser lubricant oil. This distinction can be attributed to the higher viscosity of lubricant oil, rendering water's penetration more challenging in contrast to cooking oil, which boasts a comparably lower density.

Additionally, the outcomes unveil the tangible impact of the density disparity between Fluid 1 and Fluid 2 on the stratification phenomenon. This density contrast gives rise to a substantial pressure gradient, further accentuating the velocity prompted by the gradient. Consequently, the fluid experiences an accelerated movement underpinned by this amplified pressure gradient-induced velocity.

The findings presented above unveil a comprehensive understanding of the intricate

stratification behaviors exhibited by different fluid variations. Through meticulous simulations and comparisons with experimental data, it becomes evident that the Finite Volume Particle (FVP) method adeptly captures the essence of these phenomena. The close alignment between simulation and experiment attests to the method's fidelity in reproducing real-world dynamics. The result shows good agreement with the MPS simulation, which relies on the particle method (13,14).

Interestingly, the observed time discrepancies in achieving stratification among the fluid variants underscore the nuanced influence of viscosity. Specifically, in instances where lubricant oil is involved, the extended stratification time indicates the formidable barrier posed by higher viscosity. On the other hand, the relatively quicker stratification in cooking oil points to its lower viscosity, facilitating swifter water penetration.

Moreover, the density differentiation between Fluid 1 and Fluid 2 significantly contributes to the stratification process. The density-induced pressure gradient, a pivotal driving force, triggers an escalation in velocity. Consequently, the fluid movement intensifies, propelled by the synergistic effects of pressure gradient and velocity amplification.

This study showcases the FVP method's prowess in deciphering intricate stratification phenomena and underscores the intricate interplay of factors such as viscosity and density gradients. These revelations establish a sturdy groundwork for extended investigations and practical applications within fluid dynamics and its affiliated domains. Future endeavors should encompass simulations to explore potential vortex phenomena (15,16).

CONCLUSION

In this comprehensive study, we conducted simulations to unravel inherent stratification dynamics in immiscible liquids, using the Finite Volume Particle (FVP) method to meticulously explore stratification patterns across three distinct variations. Our comparison of simulation results with prior experiments showcased remarkable alignment, emphasizing the method's proficiency in mirroring real-world phenomena. The study underscores the pivotal roles of fluid viscosity and density differentials between the two fluids in shaping velocity and temporal stratification, with higher viscosity influencing penetration dynamics. Notably, our simulations harmoniously validate experimental observations, reinforcing the FVP method's robustness in decoding stratification, particularly within molten reactor core conditions, thus advancing both method applicability and understanding of intricate fluid system stratification.

ACKNOWLEDGEMENTS

The authors wish to thank Professor K. Morita of Kyushu University for providing the basic FVP code for fluids.

REFERENCES

1. Journeau C, Bonnet JM, Boccaccio E, Piluso P, Monerris J, Breton M, et al. European experiments on 2-D molten core concrete interaction: Hecla and vulcano. Nucl Technol. 2010;170(1):189–200.
2. Salay M, Fichot F. Modelling of Metal-Oxide Corium Stratification in the Lower Plenum of a Reactor Vessel. Uranium. 2005;(33):1–17.
3. Tarantino M, Agostini P, Benamati G, Coccoluto G, Gaggini P, Labanti V, et al. Integral Circulation Experiment: Thermal-hydraulic simulator of a heavy liquid metal reactor. J Nucl Mater [Internet]. 2011;415(3):433–48. Available from: http://dx.doi.org/10.1016/j.jnucmat.2011.04.033
4. Hidayati AN, Waris A, Andi Mustari AP, Apriani NA, Ifthacharo M, Wulandari R. The Effect of Temperature Variations on Wood's Metal Plate Melting Simulation by Using MPS. J Phys Conf Ser. 2020;1493(1):0–7.
5. YuLianto Y, Hidayati AN, Mustari APA, Ilham M, Pramuditya S. Moving Particle Semi-implicit (MPS) Utilization in Analyzing the Stratification Behavior of Immiscible Liquid. IOP Conf Ser Mater Sci Eng. 2018;407(1):0–9.
6. Tran CT, Kudinov P, Dinh TN. An approach to numerical simulation and analysis of molten corium coolability in a boiling water reactor lower head. Nucl Eng Des. 2010;240(9):2148–59.
7. Irfan M, Humolungo I, Pramutadi A, Mustari A. Comparison of Melted Corium Relocation during Severe Accident of High Temperature Reactor using Moving Particle Semi-Implicit Method. 2023;6(1):1–13.
8. Hidayati AN, Waris A, Mustari APA, Irwanto D, Aprianti NA. Moving particle semi-implicit simulation on the molten Wood's metal downward relocation process. Nucl Sci Tech [Internet]. 2021;32(8):1–12.

Available from: https://doi.org/10.1007/s41365-021-00922-x

9. Wulandari R, Sutanto S, Mustari APA. Interaction of Molten Uranium With Electrical Penetrating Tube of a Boiling Water Reactor During Severe Accident. GANENDRA Maj IPTEK Nukl. 2020;23(2):55.
10. Mustari APA, Iksal I, Sumiati S. MPS simulation on melt penetration of CAFÉ experiment at 1200 C. Indones J Phys [Internet]. 2012;23(1):23–5. Available from: https://ijphysics.fi.itb.ac.id/index.php/ijp/article/view/260
11. Aprianti NA, Oshima W, Morita A, Morita K. Analysis of heat transfer behaviors in EAGLE ID1 test using particle-based simulation method. Mem Fac Eng Kyushu Univ. 2014;74(1):1–23.
12. Li G, Oka Y, Furuya M, Kondo M. Experiments and MPS analysis of stratification behavior of two immiscible fluids. Nucl Eng Des [Internet]. 2013;265:210–21. Available from: http://dx.doi.org/10.1016/j.nucengdes.2013.09.006
13. Yulianto Y, Mustari APA, Baliana A. the Stratification Behavior of Reactor Materials in the Framework of Moving Particle Semi-Implicit. J Sains dan Teknol Nukl Indones. 2022;22(2).
14. Yulianto Y, Ilham M, Pramutadi A, Matematika F, Alam P, Bandung IT. Analisis Sifat Stratifikasi Cairan Immiscible Dengan Menggunakan Metode Moving Particle Semi-Implicit (MPS).
15. Gushchin VA, Matyushin P V. Simulation and study of stratified flows around finite bodies. Comput Math Math Phys [Internet]. 2016 Jun 24;56(6):1034–47. Available from: http://link.springer.com/10.1134/S0965542516060142
16. BRUCKER KA, SARKAR S. A comparative study of self-propelled and towed wakes in a stratified fluid. J Fluid Mech [Internet]. 2010 Jun 10;652:373–404. Available from: https://www.cambridge.org/core/product/identifier/S0022112010000236/type/journal_article